REPORT DOCUMENTATION PAGE

AFRL-SR-BL-TR-98-

Public reporting burden for this collection of information is estimated to average 1 hour per response, including
and maintaining the data needed, and completing and reviewing the collection of information. Send comm
information, including suggestions for reducing this burden, to Washington Headquarters Services, Directorate
1204, Arlington, VA 22202-4302, and to the Office of management and Budget, Paperwork Reduction Project ((

0736

gathering
lection of
ray, Suite

1. AGENCY USE ONLY (Leave Blank)	2. REPORT DATE December, 1991	3. REPORT TYPE AND DATES COVERED Final

4. TITLE AND SUBTITLE Excimer Laser Deposition of PLZT Thin Films	5. FUNDING NUMBERS

6. AUTHORS
Gary Allen Petersen, Jr.

7. PERFORMING ORGANIZATION NAME(S) AND ADDRESS(ES) University of New Mexico	8. PERFORMING ORGANIZATION REPORT NUMBER

9. SPONSORING/MONITORING AGENCY NAME(S) AND ADDRESS(ES) AFOSR/NI 4040 Fairfax Dr, Suite 500 Arlington, VA 22203-1613	10. SPONSORING/MONITORING AGENCY REPORT NUMBER

11. SUPPLEMENTARY NOTES

12a. DISTRIBUTION AVAILABILITY STATEMENT Approved for Public Release	12b. DISTRIBUTION CODE

13. ABSTRACT *(Maximum 200 words)*

See Attachment

14. SUBJECT TERMS

15. NUMBER OF PAGES

16. PRICE CODE

17. SECURITY CLASSIFICATION OF REPORT Unclassified	18. SECURITY CLASSIFICATION OF THIS PAGE Unclassified	19. SECURITY CLASSIFICATION OF ABSTRACT Unclassified	20. LIMITATION OF ABSTRACT UL

DTIC QUALITY INSPECTED 3

Standard Form 298 (Rev. 2-89)
Prescribed by ANSI Std. 239.18
Designed using WordPerfect 6.1, AFOSR/XPP, Oct 96

GARY ALLEN PETERSEN, JR.

Candidate

ELECTRICAL AND COMPUTER ENGINEERING

Department

This thesis is approved, and it is acceptable in quality
and form for publication on microfilm:

Approved by the Thesis Committee:

_____ , Chairperson

_____

_____

_____

_____

_____

_____

_____

Accepted:

_____
Dean, Graduate School

_____
Date

EXCIMER LASER DEPOSITION OF PLZT THIN FILMS

BY

GARY ALLEN PETERSEN, JR.

B.S. Physics, Rensselaer Polytechnic Institute, 1989

THESIS

Submitted in Partial Fulfillment of the
Requirements for the Degree of

Master of Science in Electrical Engineering

The University of New Mexico
Albuquerque, New Mexico

December 1991

Acknowledgements

I would like to express my thanks and appreciation to the following people for their encouragement and support throughout this endeavor.

To my advisor Dr. John R. McNeil for his advice, ideas and patience, and without whom, none of this would have been possible.

To my coworkers, especially Leonard Boyer, David Reicher, Chris Kranenberg, and Dr. Scott Wilson for their advice and ingenuity in helping me to find answers to my numerous questions.

To Mark Miller from the UNM Department of Geology for his assistance in obtaining and analyzing the x-ray diffraction results.

To Rick "The Option Man" Myers for his constant ability to aid me in pursuing the most logical direction to follow.

To Dr. Forrest "Flanders" Williams for insight into our "common denominator" and for giving me motivation and cause to proceed.

To my family, my parents for their undying love and support, and my brother, for whom I have the utmost respect and admiration.

ABSTRACT

Excimer Laser Deposition of PLZT Thin Films

Gary Allen Petersen, Jr.

B.S. Physics, Rensselaer Polytechnic Institute, 1989

M.S. Electrical Engineering, University of New Mexico, 1991

Laser ablation has been used to produce thin films of lanthanum-modified lead zirconate titanate or PLZT, as defined by $Pb_{1-x}La_x(Zr_{1-y}Ti_y)_{1-x/4}O_3$. PLZT is an interesting class of materials having a wide range of compositionally dependent electrooptical properties and strong non-linear optical characteristics.

PLZT is highly transparent in the infrared and visible spectral regions with a UV band edge occurring at approximately 300 nm. Therefore, opportunities for applications of PLZT thin films for electronic and optoelectronic devices are numerous. Such proposed devices include optical switches, optical modulators, thin film waveguides, and nonvolatile memory devices. In order to integrate these devices into optical systems, the production of high quality thin films with high transparency and perovskite crystal structure is desired. This requires development of deposition technologies to overcome the challenges of depositing and processing PLZT thin films.

This thesis examines the deposition of PLZT thin films by excimer laser ablation. PLZT thin films of 7/0/100, 28/0/100, and 0/0/100 compositions, as denoted by (x/1-y/y)*100 from the chemical formula, have been deposited onto crystalline Si <100> and amorphous fused silica substrates. The stoichiometry, crystallinity, and grain sizes of the deposited films were determined. Effects of oxygen backfill pressure were also investigated. The results indicate that laser ablation provides the ability to deposit stoichiometrically correct PLZT thin films with high deposition rates and perovskite crystal structure. Hence, laser ablation provides a suitable technique for PLZT thin film deposition.

Table of Contents

List of Figures

List of Tables

CHAPTER 1

INTRODUCTION

Lanthanum-modified lead zirconate titanate, or PLZT, given by the chemical formula $Pb_{1-x}La_x(Zr_yTi_{1-y})_{1-x/4}O_3$ is a well known ferroelectric material having various pronounced electrooptic and piezoelectric properties. These properties may be selected by altering the stoichiometric composition of the material.[1] By adjusting the composition, PLZT can be made into transparent ferroelectric materials for electronic and optoelectronic device applications.[2] These materials include films with perovskite crystal structure, low optical scatter, and high transparency. The PLZT crystal is nearly centrosymmetric in the paraelectric phase but has a distorted centrosymmetry in the ferroelectric phase.[16] This allows for strong non-linear optical effects since χ^2 and χ^3 are non-zero in the ferroelectric phase. The most significant obstacle in obtaining good transparency and electrooptic properties is developing material with perovskite structure and large grain size on suitable substrate materials.[3] This problem poses an interesting challenge in depositing and processing PLZT thin films.

1.1   Ferroelectric Materials

Ferroelectric crystals are characterized by a net spontaneous polarization, P_s, caused by a noncentrosymmetric arrangement of ions in the unit cell resulting in an associated electric dipole

moment.[4] P_s may be reoriented in terms of certain atomic motions by applying an electric field, thereby changing the polar direction.[5] Crystal axis elongation is a distortion of the unit cell caused by acentric symmetry. Domains are formed by adjacent unit cells that distort in a similar manner.

Applying large electric fields to ferroelectric materials causes domains oriented in the field direction to grow at the expense of other domains. This process is increased until no further growth or reorientation occurs with increased electric field. The material is then said to have a saturated polarization, P_{sat}. If the field is removed, the domains do not return to their original position but remain in their new "poled" condition. The material is now said to have a saturated remnant polarization, P_r, which may be switched to intermediate values by reapplying an electric field.[4]

Ferroelectric materials possessing electrooptic properties are usually transparent or semi-transparent and polycrystalline. Typical grain sizes range from <0.5-50 μm depending on chemical composition and fabrication technique.[4]

1.2 Physical Properties of PLZT

Lead-zirconate titanate [Pb(ZrTi)O$_3$], or PZT, compositions were the first electrooptic ceramics to receive a great deal of research attention. Their compositionally dependent

2

optoelectronic properties make them highly interesting. Because of their polycrystalline nature, they exhibit a large amount of optical scatter which leads to increased optical loss. This is undesirable in optical and electrooptical systems. By introducing lanthanum into PZT materials, index of refraction discontinuities at domain boundaries are decreased,[7] resulting in decreased optical scatter and higher transparency. This also improves the switching and optical properties of the material.[4] Other elements such as boron, tin, and bismuth have been substituted for the lanthanum to improve the material properties,[7] but PLZT outperformed all other modified PZT materials for electrooptic applications.

PLZT is an ABO_3 perovskite similar to $BaTiO_3$. The ABO_3 perovskite structure is shown in Figure 1.1. This is a tetragonal structure with a transition metal (Zr or Ti) at the center surrounded by an oxygen octahedra and alkaline atoms (Pb or La) at the corners. The structure shown in Figure 1.1 is appropriate for temperatures at or above the Curie point. As the temperature is lowered below this point, the titanium ion is displaced from its body-centered position towards one of the face centers. The cubic unit cell also deforms and becomes tetragonal. The net charge of the titanium ion causes the unit cell to acquire a dipole moment in the direction of the titanium displacement.[6]

PLZT

Pb, La   **O**   **Zr, Ti**
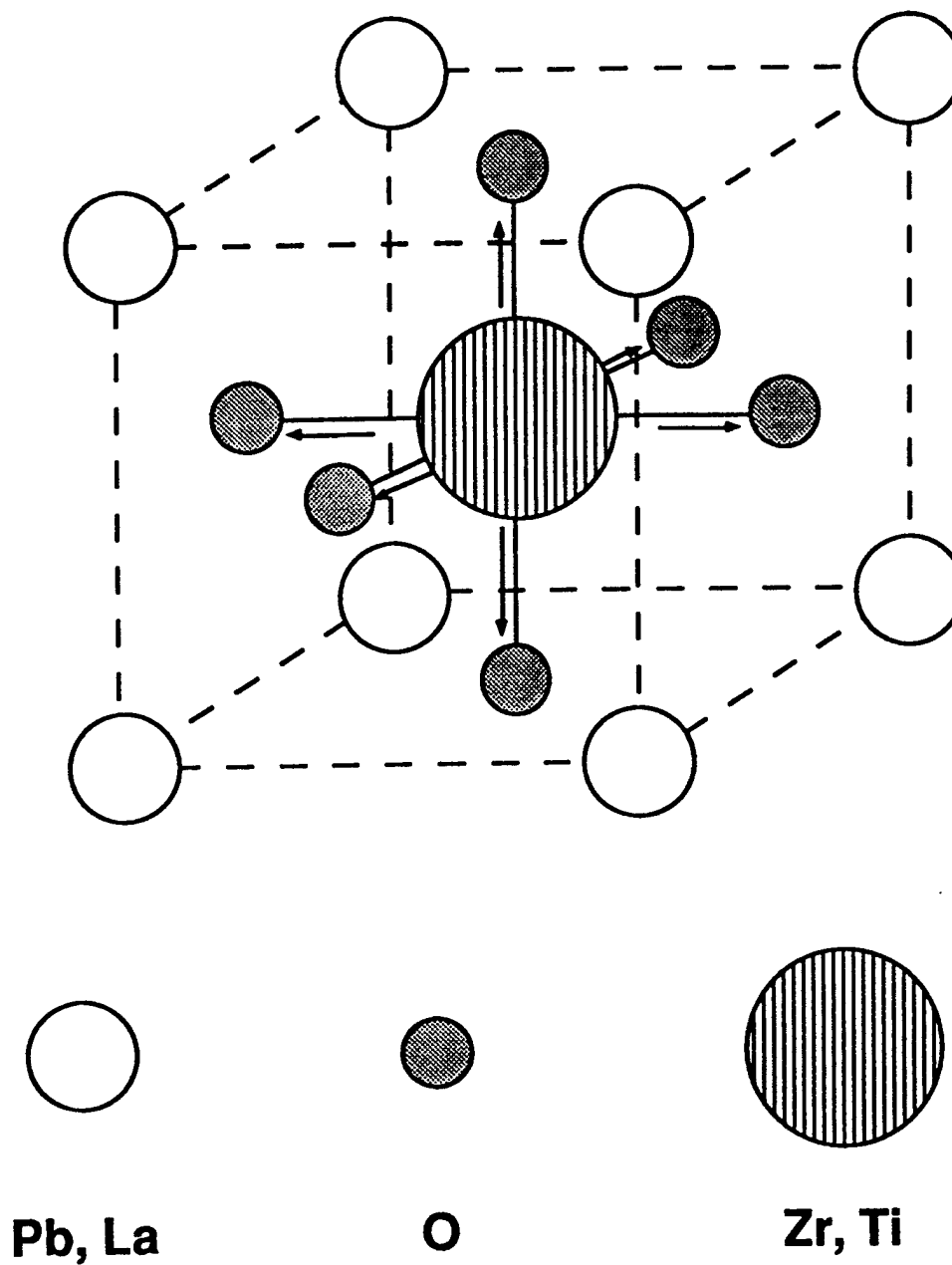
Figure 1.1:   Perovskite structure PLZT unit cell.

The optoelectronic properties exhibited by PLZT are: electrooptical memory effects (remnant polarization), linear electrooptic effects (Pockels effect), and quadratic electrooptic effects (Kerr effect).[4] When light propagates normal to the applied electric field, these properties are labeled as transverse electrooptic effects. These effects are dependent upon both the La content and the Zr:Ti ratio of the material.[6]

1.3 Optical Behavior

High quality PLZT is transparent in the infrared and visible spectral regions. Depending on the material composition, the UV absorption band edge occurs at approximately 300 nm. There have been numerous proposals for PLZT applications in electronic and optoelectronic devices. Electronic device applications include a non-volatile memory FET with a ferroelectric gate[10] and image storages[13] which make use of the remnant polarization. Optical applications are optical switches[11], optical modulators[12], and optical display devices[14] which make use of the fast switching times of the material. The transparency of PLZT allows for good thin film waveguides[15], and a large χ^3 makes optical harmonic generation possible.[16]

The index of refraction of PLZT is approximately 2.5 at $\lambda=632$ nm. Unfortunately PLZT displays a considerable amount of dispersion which can influence the use of this material in waveguiding and harmonic generation applications. Also, the

optical behavior of ferroelectric ceramics is dependent upon the individual grain properties. The size and orientation of the grains affect both the linear and non-linear optical behavior of the material.[4]

Device fabrication might require several post-deposition processes such as annealing and etching. Because of the nature of the PLZT crystal, post deposition processing of the material is very difficult. The polycrystalline nature of the PLZT material causes irregular etching of domains in most etching processes, leading to increased optical scatter in the material. Also, each additional post processing step incurs larger cost requirements. This presents a need to improve post processing techniques.

Several techniques have been used to deposit ferroelectric thin films such as RF and DC magnetron sputtering, electron beam evaporation, solution-gelatin (sol-gel) processes, and ion beam sputtering.[4] The challenges present in ferroelectric film fabrication, such as multicomponent composition and phase control, are similar to those encountered in the deposition of high temperature superconducting materials. This makes laser ablation an attractive approach to in-situ thin film growth.

Each of the aforementioned techniques has resulted in films with perovskite structure, yet each process has its advantages and disadvantages. The disadvantages range from lower adatom

energies in magnetron sputtering, uniformity problems in sol-gel films, lower deposition rates for ion beam sputtering[4], and the need for post-deposition annealing to obtain correct crystalline srtuctures and incorporate oxygen into the films. In-situ deposition of oriented PLZT thin films via laser ablation would yield a desirable improvement in film quality.

The following thesis will summarize the investigation of laser deposited PLZT thin films. Chapter 2 describes the experimental procedure and characterization techniques used to analyze the films. Chapter 3 describes the results obtained from the characterization methods. Chapter 4 discusses those results, and Chapter 5 draws conclusions from the results and proposes areas in which future investigation might be done to improve understanding of the laser deposition process.

CHAPTER 2

EXPERIMENTAL PROCEDURE

In this investigation laser ablation was used to deposit PLZT thin films of composition 7/0/100, 28/0/100, and 0/0/100 (lead titanate) onto crystalline Si <100> and amorphous fused silica substrates. The goal of this work was to develop a process to successfully deposit PLZT using laser ablation. The results of this process will be compared to other deposition techniques. The compositions investigated contained no zirconium. Zirconium enhances the electronic and memory properties of the material by creating large remnant polarizations and decreases the transparency because of optical absorption. The optical properties are stronger in the PLT compositions.

2.1 Film Deposition

Evaporation techniques typically yield adatoms of low energy (~0.1 eV) and usually require high substrate temperatures (≥ 500 °C) to produce high quality films.[4] Sputtering techniques typically yield adatoms of energies ~1-10 eV.[17] Laser ablation yields even higher adatom energies (~10-50 eV).[18] Energies as high as 80 eV have been reported.[19]

The higher adatom energies provided by sputtering and laser ablation techniques tend to create higher quality films

compared to evaporated films.[9, 20] This is believed to be due to the increased mobility of the adatom on the surface of the substrate.[8,9] This increased mobility allows the adatom to seek out and find the local minimal potential energy sites, thereby forming denser films. This increased surface mobility helps to form good crystalline structures at lower substrate temperatures. Lower substrate temperatures are often desired to deposit films on certain substrates. The combination of higher adatom energies with lower substrate temperatures can produce high quality PLZT thin films having good crystallinity and desirable nonlinear optical properties.[4]

Deposition rates for depositing dielectric and ferroelectric materials are high (1-1000 Å/sec), except for ion beam sputtering. Ion beam sputtering typically yields deposition rates on the order of 0.1-2 Å/sec.[4] Deposition rates for laser ablation are most dependent on the pulse rate of the laser. For example, one group reported a deposition rate of $\approx$150 Å/sec with a pulse rate of 1000 Hz.[20] In this investigation a pulse rate of 10 Hz was used to produce a deposition rate of 1-2 Å/sec.

2.2 Laser Ablation

Laser ablation is a suitable technique for investigating the deposition of thin films of dielectric and ferroelectric materials at the laboratory scale. Laser ablation utilizes the energy of a laser to vaporize a source material. The depth at which the incident

energy is absorbed varies from a few hundred angstroms to several centimeters depending upon the target material's optical properties and bandgap, and the operating parameters of the laser such as wavelength, energy, and pulse rate.[21] A high energy laser beam incident on a target surface produces a plume of material that can be directed at a substrate to grow films of the desired material. The earliest studies of interactions between high energy lasers and materials concerned damage to laser optics and solid state crystals.[22] Laser ablation was first used intentionally in the production of optical dielectric coatings.[23] Since then, laser-induced processes have been utilized to produce high quality thin films of optical and piezoelectric materials,[21,24] epitaxial semiconductor layers,[25] synthetic diamond,[26] and recently, high-transition temperature superconductors.[27,28,29]

Laser ablation has a number of advantages as a physical deposition source. These include the production of stoichiometric films, high energy atomic and molecular species, directed deposition, and wide applicability. Perhaps the most impressive advantage offered by laser ablation is the congruent evaporation of many components from a single target. This arises from the fact that non-equilibrium laser induced heating (10^{11} K/s) and rapid cooling of the near surface layer typically occurs on a time scale t<<1 ms that is much shorter than the time required for diffusion or segregation of material in the laser heated zone. Thus

physical processes such as evaporation or sputtering may occur stoichiometrically.[20]

Laser desorption from the target under high intensity (plasma-forming) conditions can also produce a variety of high energy atoms, molecules, fragments, and ions, resulting in local annealing and improved crystalline structure of the films at the substrate.[30] The angular distribution of the laser-generated plume is described by a $\cos^n(\Theta)$ distribution where $1 \leq n \leq 8$.[31] The directed plume is partly explained on the basis of hydrodynamic flow and can be used to coat a variety of shapes and sizes of objects, similar to a directed spray gun.[32,33]

Various types of pulsed lasers have been used as ablation sources, including CO_2, Nd:YAG, and excimer lasers. However, pulsed excimer laser deposition has emerged as the method of choice because of the shorter penetration depth of the UV radiation, availability of high average powers, and spatial uniformity of the beam intensity profile. This investigation used a KrF excimer laser operating at 248 nm.

2.3 Target Fabrication

Laser ablation is a process where pulsed laser light is focused onto a target of the desired deposition material. In general, any target material that can be physically held in vacuum

and strongly absorbs light at the wavelength of the laser can be used for ablation.

Circular 2"-diameter targets were used for this investigation. The powder was prepared using the individual component oxides PbO, TiO$_2$, and La$_2$O$_3$. Using the following expression

$$Pb_{1-x}La_x(Zr_{1-y}Ti_y)_{1-x/4}O_3 \qquad (2.1)$$
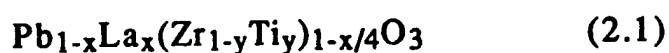
and the phase diagram of Figure 2.1, the desired composition and corresponding film properties could be selected. From this, the necessary amount of required oxides for a target could be calculated. Table 2.1 shows the amounts needed to produce ≈150 grams of target material for the various compositions.[4]

During the deposition process much of the lead is lost due to the reduced sticking and accommodation coefficients at elevated deposition temperatures.[40] Therefore excess PbO must be added to the targets during the material preparation. The excess PbO amounts were determined empirically and are shown in Table 2.1.

The oxides were placed in a nalgene container with zirconia grinding pellets and 111-Trichloroflouroethane (freon). The composition was mixed and ground for 24 hours to produce a well mixed, finely ground slurry. The slurry was placed in a stainless steel pan and heated to 150 °C to evaporate the freon. The dried
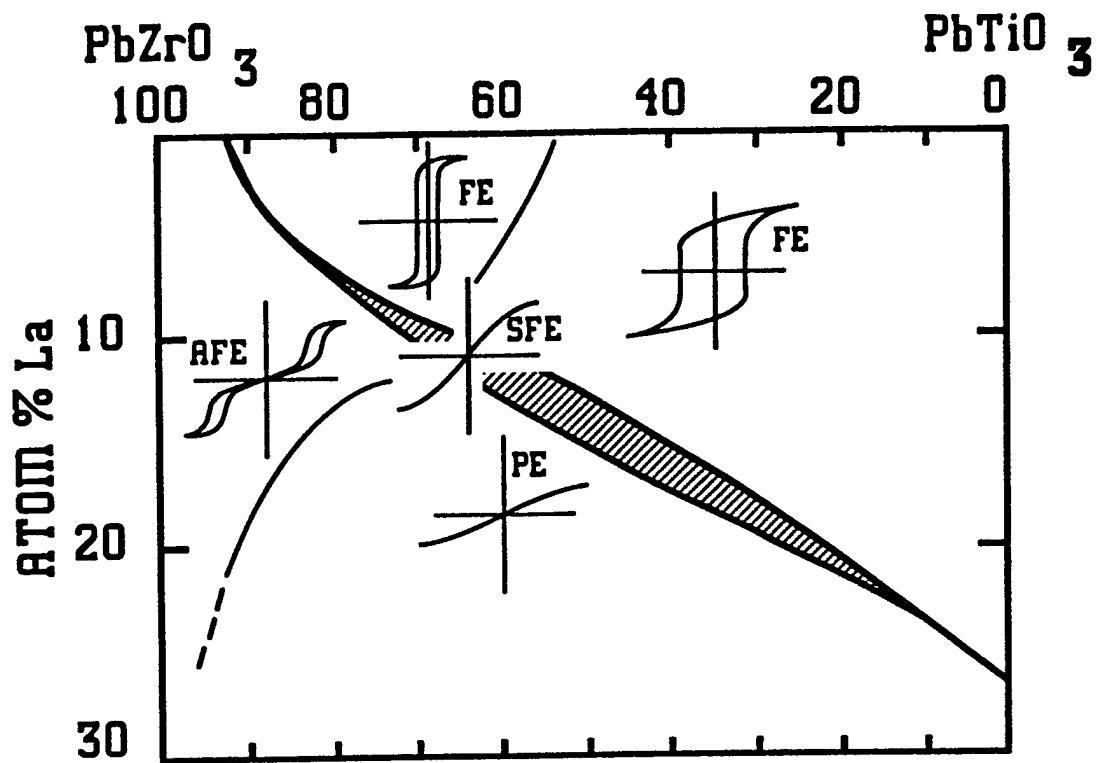
Figure 2.1:   PLZT Phase Diagram

Film Composition	PbO content	La$_2$O$_3$ content	TiO$_2$ content	ZrO$_2$ content
7/0/100	103.779g	5.701g	39.241g	0g
Excess PbO %				
75%	181.613g	5.701g	39.241g	0g
100%	207.558g	5.701g	39.241g	0g
28/0/100	85.90g	24.38g	39.715g	0g
Excess PbO %				
75%	150.325g	24.38g	39.715g	0g
100%	171.80g	24.38g	39.715g	0g
0/0/100	75.0g	0g	75.0g	0g
Excess PbO %				
75%	131.25g	0g	75.0g	0g
100%	150.0g	0g	75.0g	0g

Table 2.1:   PLZT Target Composition

powder was placed in an Al_2O_3 crucible and sintered at 900 °C for 9 hours. This allowed the lanthanum to become hygroscopically stabilized within the material. Without stabilization, the target would absorb H_2O and increase in volume due to the lanthanum affinity for H_2O.[4] A mortar and pestle were used to grind the sintered material into a fine powder. The powder was placed into a 2" stainless steel target holder and pressed flat by using a 25 ton press for 15-20 minutes. The target holder maintained the structural integrity of the target and provided ease of installation and removal from the vacuum chamber. After pressing the material into the holder, the target holder was mounted onto a rotating shaft inside the vacuum chamber.

2.4   Substrate Preparation

In this investigation, substrates of silicon <100> wafers and amorphous fused silica were used. Each substrate was cleaned carefully prior to mounting in the vacuum chamber for deposition. The cleaning process for the silicon and fused silica substrates consisted of several steps.

The silicon substrates were placed in a 3 parts semiconductor grade H_2O_2 : 2 parts H_2SO_4 solution. This was done to grow an SiO_2 layer at the silicon-oxide interface, thereby removing any Si contaminants to the oxide layer. The silicon substrates were placed in a 5% HF: deionized (DI) H_2O etch for ≈ 5 minutes to remove the SiO_2 layer and leave the clean silicon

surface. The substrates were removed from the etch and placed onto the substrate holder in the vacuum chamber.

The fused silica substrates were placed into the 3:2 H_2O_2:H_2SO_4 solution for a few minutes to remove any organic contaminants from the surface. The substrates were scrubbed using a soft bristle brush with Liquinox soap and DI water several times. This was followed by a rinse with DI water, acetone, and ethyl alcohol to remove the residual soap. Finally, the fused silica substrates were drag wiped with ethyl alcohol and lens tissue, blown off with nitrogen, and inspected with high intensity light for cleanliness before being placed into the vacuum chamber. After loading the substrates onto the stainless steel substrate holder and sealing the vacuum chamber, the chamber was evacuated to a base pressure of $\approx 2 \times 10^{-7}$ Torr.

2.5   Film Deposition Parameters

PLZT thin films were deposited using targets containing excess amounts of lead oxide within a 23 inch vacuum chamber. Figure 2.2 illustrates the experimental configuration for this investigation.

A KrF excimer laser was operated at a wavelength of 248 nm with a pulse rate of 10 Hz and a pulse width of 20 ns. For this investigation a spot size of ~3 mm^2 was used. The light was focused onto the target using two lenses and a turning mirror
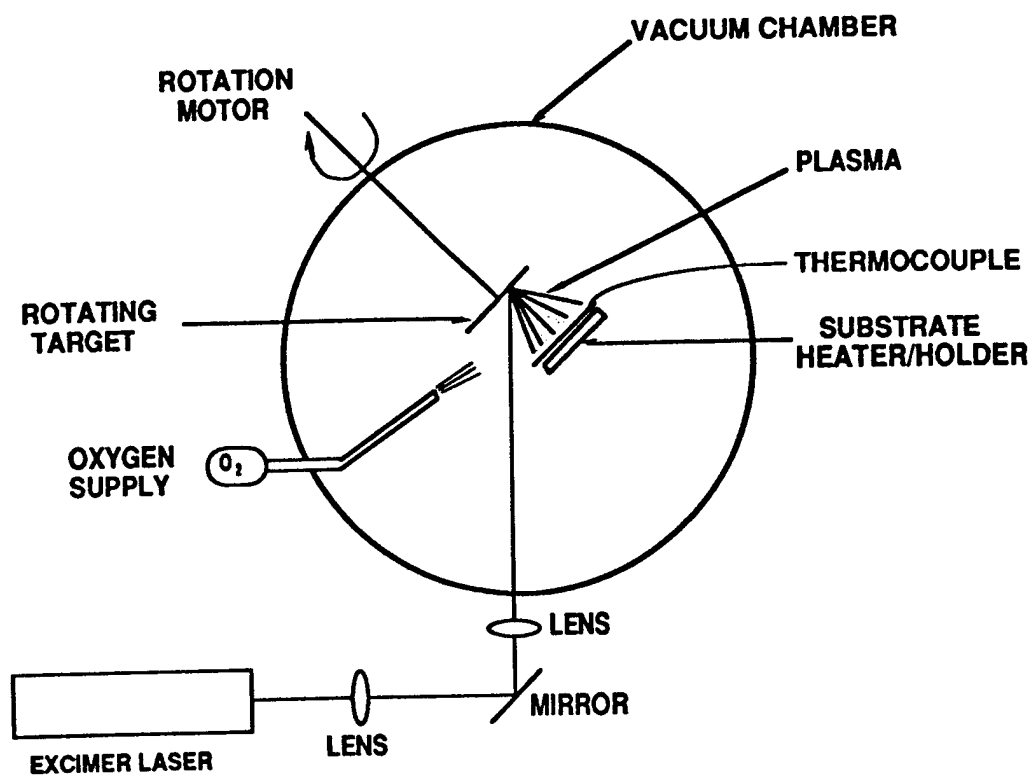
SCHEMATIC OF PLZT LASER ABLATION SYSTEM

Figure 2.2:   Laser Ablation Chamber Configuration

outside the vacuum chamber. The energy density of the light incident upon the target could be altered by changing the distance between one of the lenses and the target, thereby changing the spot size of the incident beam. The laser beam had an angle of incidence of approximately 45° with respect to the normal of the target.

The target was mounted on a rotating shaft which operated at ≈5 rpm. The substrates were mounted parallel to the target on a stainless steel plate which directly contacted a resistively heated ceramic plate capable of temperatures up to 1000 °C. Substrate temperatures ranged from 400-650 °C. The substrate temperature was raised quickly (10-15 minutes) to the desired deposition temperature and held constant (+/- 5 °C) throughout the deposition using a Type J thermocouple and temperature controller. The heater was allowed to cool to room temperature over a period of approximately 2 hours. The slow cooling rate prevented film crazing due to thermal shock and differences in PLZT/substrate thermal expansion coefficients.

To investigate uniformity, stoichiometry, and deposition rates, the target-substrate separation was varied from 4 to 8 cm. The substrate temperature varied between 400 and 500 °C. The vacuum chamber was backfilled with oxygen to a pressure of 0.2 mTorr.

Another part of the investigation consisted of examining the stoichiometry as a function of oxygen backfill pressure and excess lead oxide in the target. For these experiments the target-substrate separation was held constant at 6 cm. Oxygen pressure during deposition was varied between 0.1 and 200 mTorr. The substrate temperature ranged between 500 and 530 °C for these experiments. The deposition parameters for the two studies are shown in Tables 2.2 and 2.3, respectively.

2.6   Film Analysis

Several techniques were used to analyze the deposited thin films. Energy dispersive x-ray spectrometry (EDS) determined stoichiometry, X-ray diffraction (XRD) determined crystallinity, and scanning electron microscopy examined surface morphology and structure. Optical transmittance, index of refraction, and nonlinear optical properties can be used to further characterize PLZT thin films.

2.6.1   Film Stoichiometry

The crystal structure, optical and electronic properties of PLZT thin films are strongly dependent upon the composition of the film. EDS was used to measure the ratios of Pb:Ti, Pb:La, and Ti:La in the laser deposited films. EDS is a technique utilizing x-rays produced from a sample being bombarded with electrons. The x-rays are passed through a beryllium window onto a reverse biased p-type - intrinsic - n-type (p-i-n) silicon detector.

19

PLZT Target Composition	7/0/100 (+ excess PbO)
	28/0/100 (+ excess PbO)
Substrate Material	Si <100>
	Fused Silica
Target-Substrate Separation	4 - 12 cm
Laser Wavelength	248 nm
Substrate Temperature	400 - 500 °C
Oxygen Backfill Pressure	0.2 mTorr
Energy Density	5 J / cm^2
Deposition Rate	1 - 2 Å / sec

Table 2.2:   Deposition Parameters - Part 1

PLZT Target Composition	7/0/100 (+ excess PbO)
	28/0/100 (+ excess PbO)
	0/0/100 (+ excess PbO)
Substrate Material	Si <100>
	Fused Silica
Target-Substrate Separation	6 cm
Laser Wavelength	248 nm
Substrate Temperature	450 - 550 °C
Oxygen Backfill Pressure	0.1 - 200 mTorr
Energy Density	5 J / cm^2
Deposition Rate	1 - 2 Å / sec

Table 2.3: Deposition Parameters - Part 2

Absorption of x-ray photons by the detector causes photoelectrons to be ejected. The photoelectrons give up most of their energy to electron-hole pairs. The pairs are collected by an applied bias to form a charge pulse which is converted to a voltage pulse by a charge preamplifier. Further processing of the signal yields a voltage distribution displayed on a CRT or a chart recorder. The voltage values displayed are correlated with data on x-ray absorption and emission to give elemental peak identification or quantification.[4] Because EDS only yields information about the existence of an element in a sample and not to compounds and phases formed with that element, the identification of elemental material composition is qualitative. An electron accelerating voltage of 20 kV allowed the electrons to pass completely through the film ($\approx$5000 Å) as evidenced by the detection of the substrate material. This insured that the entire film was examined and not the surface alone.

The best detectors available cannot detect all of the chemical elements, especially those lighter than beryllium. This is because the x-rays cannot be absorbed to eject photoelectrons in the lighter elements. In this investigation, elements lighter than sodium could not be detected with the available system. This did not present a problem since all of the metal elements in the PLZT thin films are easily detectable by EDS

2.6.2 Crystal Structure

The crystal structure of the PLZT thin films was determined with x-ray diffraction techniques. These techniques reveal the phase, unit cell dimensions, stress and strain states, and material composition.[4]

A Scintag x-ray diffractometer was used to determine the crystalline properties of PLZT thin films. The measurement configuration used was a normal scan. The normal scan configuration involved both the x-ray source and detector to rotate about the sample. X-ray diffraction data from the sample over a wide range of scattering angles was obtained. The scanning configuration gave the phases present and whether the film was perovskite or pyrochlore in structure due to correct or incorrect composition, respectively. The phases were determined by correlating the diffraction peak data with the JCPDS (Joint Committee on Powder Diffraction Systems) data base.[43]

Another scanning configuration was the 2Θ scan. Using this configuration, information about individual diffraction peaks can be determined. In the 2Θ configuration, the x-ray source remains stationary at a particular diffracted peak position or 2Θ value. The x-ray detector is rotated from 2° from the tangent of the substrate surface to 4Θ. Splitting in the chosen diffracted peak will determine the deviation of the crystal direction from the normal. This determines unit cell orientation or c-axis orientation

of the material. The 2Θ scan also provides information on unit cell dimensions along with stress and strain states.

2.6.3 Surface Structure

A scanning electron microscope (SEM) examined the surfaces of several of the PLZT thin films. The SEM measures the energies of secondary electrons and displays the energy distribution in an x-y coordinate system, thereby reconstructing the image of the sample.

SEM images of the films at high magnifications ($\approx$70 kX) were examined revealing individual grains in the films. The grain sizes of films deposited by several different techniques were compared.

CHAPTER 3

EXPERIMENTAL RESULTS

The experimental results of this investigation, obtained from the characterization techniques described in the previous chapter, will be presented. The experiment consisted of two parts. Part one examined operating parameters for the deposition process. Part two investigated stoichiometry as a function of oxygen backfill pressure. X-ray diffraction measurements (XRD), energy dispersive x-ray spectrometry (EDS), and scanning electron microscopy (SEM) were used to quantify the effects of these parameters.

3.1 Parameter Determination

Part one investigated crystallinity, stoichiometric uniformity, and deposition rates to determine optimum deposition parameters. The operating parameters are shown in Table 2.2.

3.1.1 Crystal Structure

Highly oriented PLZT thin films were obtained with laser deposition. Figures 3.1 and 3.2 illustrate the x-ray diffraction patterns of PLZT (7/0/100) deposited on Si <100> at substrate temperatures of 450 °C and 500 °C respectively.
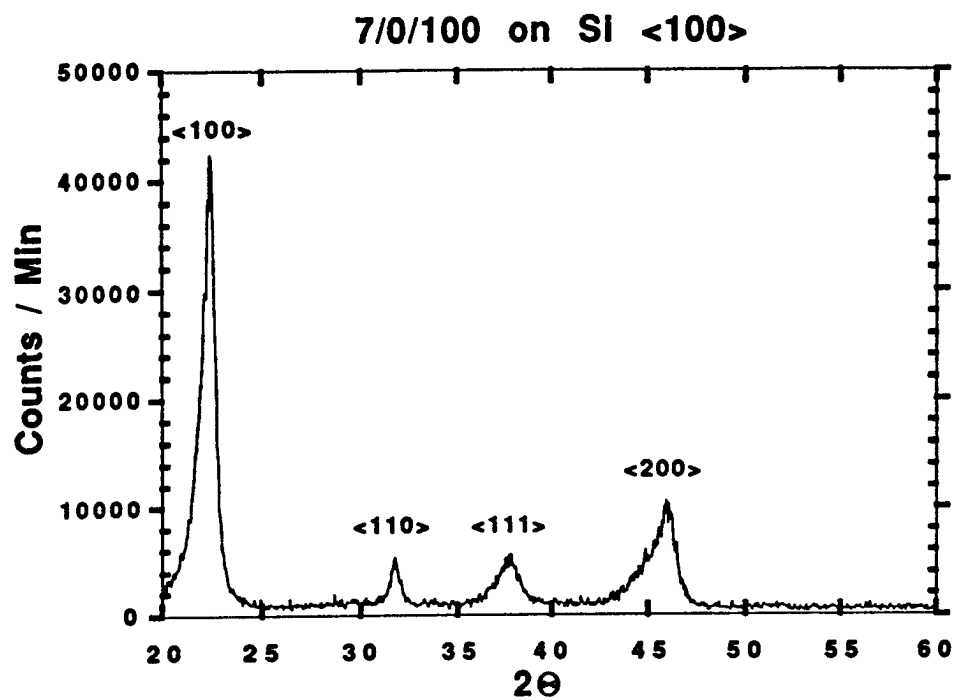
7/0/100 on Si <100>

Figure 3.1: X-Ray Diffraction Pattern of 7/0/100 PLZT on <100> Silicon @ 450 °C.
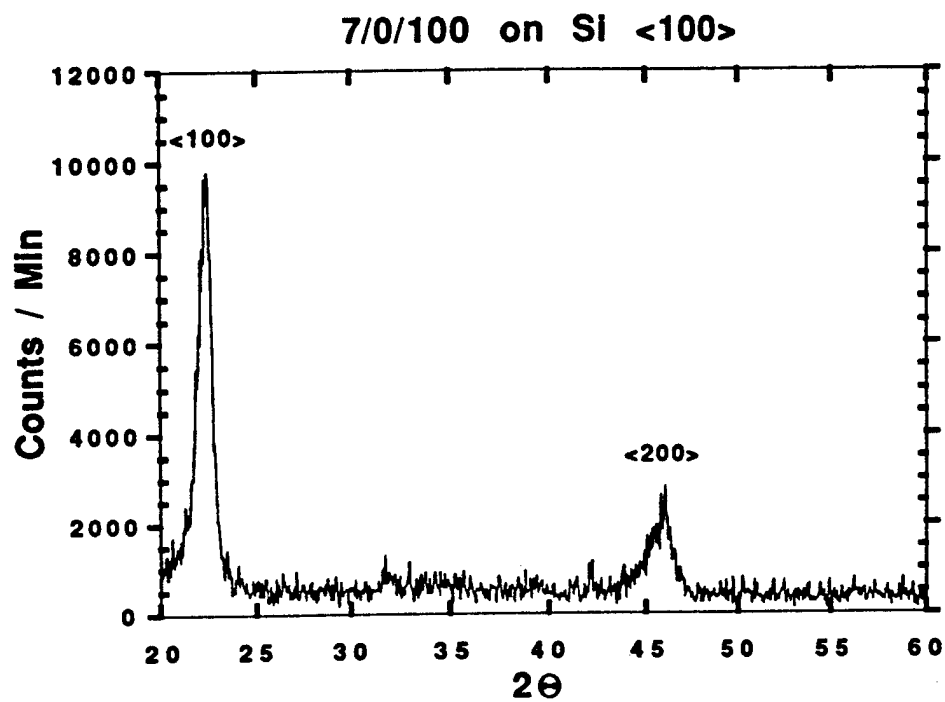
Figure 3.2: X-Ray Diffraction Pattern of 7/0/100 PLZT on <100> Silicon @ 500 °C.

Films deposited at 450 °C on Si <100> show a presence of mixed crystalline phases. Here we see the <100> and <200> peaks along with the <110> and <111> peaks at $2\Theta=31°$ and 37° respectively. The 500 °C sample illustrates the desired perovskite structure as shown by a <100> peak at $2\Theta=22.6°$ and a second order diffraction peak <200> at $2\Theta=46°$. Figure 3.3 illustrates the pyrochlore structure as evidenced by the peak at $2\Theta=29°$. This structure is typical of films deposited at lower temperatures or with lead deficiencies.

The pyrochlore structure of the material results from improper film stoichiometry and/or low deposition temperatures. It is caused by the oxygen atoms in the crystal lattice being replaced by one or more of the other elements (Pb, Ti, La, or Zr). The pyrochlore structure is undesirable for optical uses because it does not display nonlinear characteristics. By annealing films with pyrochlore structure, perovskite structure may be obtained. Note that the films represented by Figures 3.1 and 3.2 were perovskite in structure without a post-annealing process. Post-annealing is undesirable because of the additional processing step involved. Also there is an increased possibility of crazing due to the thermal expansion differences between the film and substrate.

PLZT (7/0/100) was also deposited on amorphous fused silica substrates. The as-deposited samples displayed a perovskite/pyrochlore mixed crystal structure with a pyrochlore
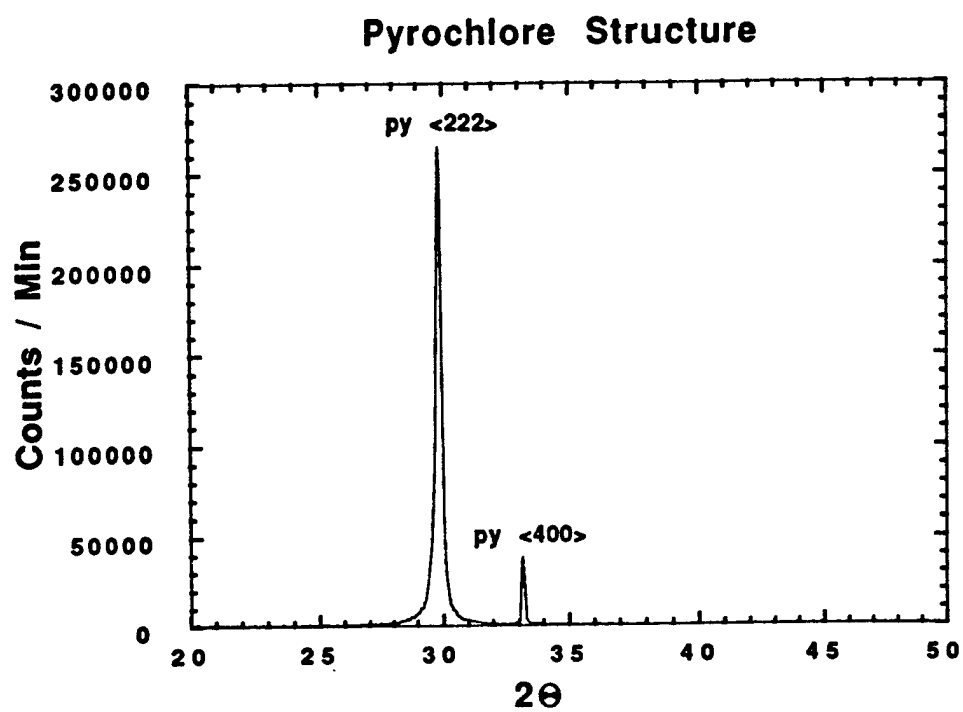
Pyrochlore Structure

Figure 3.3: PLZT with Pyrochlore Structure $(2\Theta \approx 29°)$

peak at 29°, and a <111> peak at 37° as seen in Figure 3.4. Figure 3.5 shows post-annealing of this film at 550 °C for twenty minutes improved the crystalline structure. The predominant phase of the material became <111> as the pyrochlore peak diminished and became unobservable. Again proper deposition temperature was required in order to induce correct crystal structure.

3.1.2 Stoichiometry

In this part of the investigation it was noticed that the film composition changed across the substrate. Figures 3.6 and 3.7 show the lead-to-titanium plus lanthanum, Pb/(Ti+La), ratio as a function of distance across the substrate for both the (7/0/100) and (28/0/100) target compositions respectively. For both compositions, the Pb/(Ti+La) ratio decreased slightly from the center (0 mm) to 5 mm. The 28/0/100 composition film deposited at a target substrate separation of 12 cm shows a large decrease possibly due to experimental error in either the deposition or the measurement techniques. The stoichiometry of the films remained relatively constant from 5 to 10 mm, and tended to either increase or decrease with distance for an additional 5 mm. This was due to the increased non-uniformity and decreased thickness away from the center of the film caused by the plume geometry. EDS measurements are difficult to obtain on the non-uniform and thinner areas of the films.
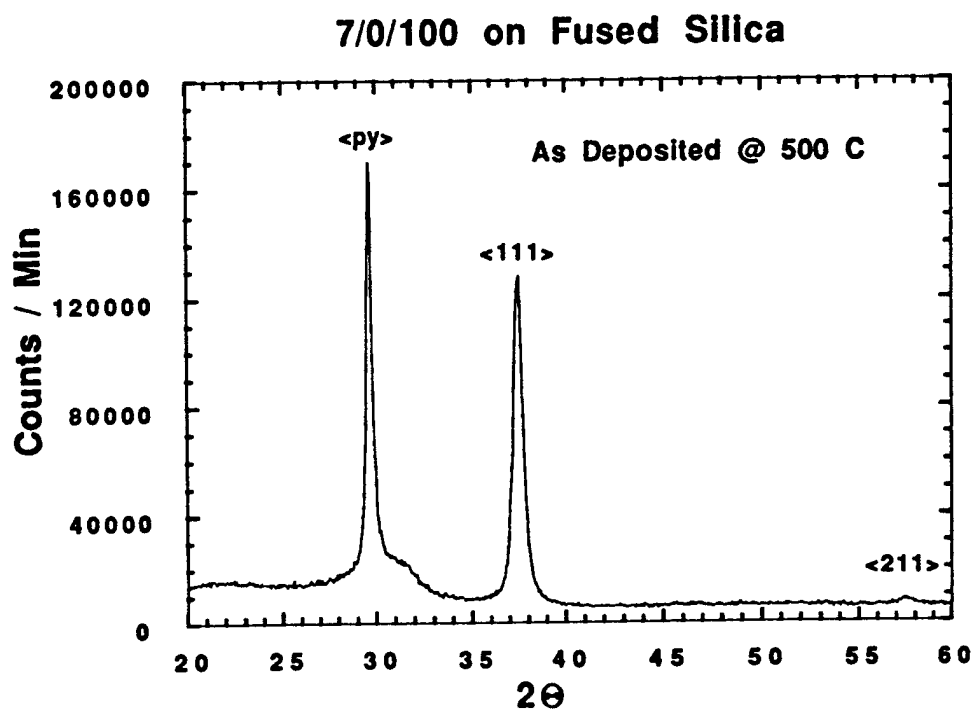
Figure 3.4: X-Ray Diffraction Pattern of 7/0/100 PLZT on Fused Silica @ 500 °C.

7/0/100 on Fused Silica
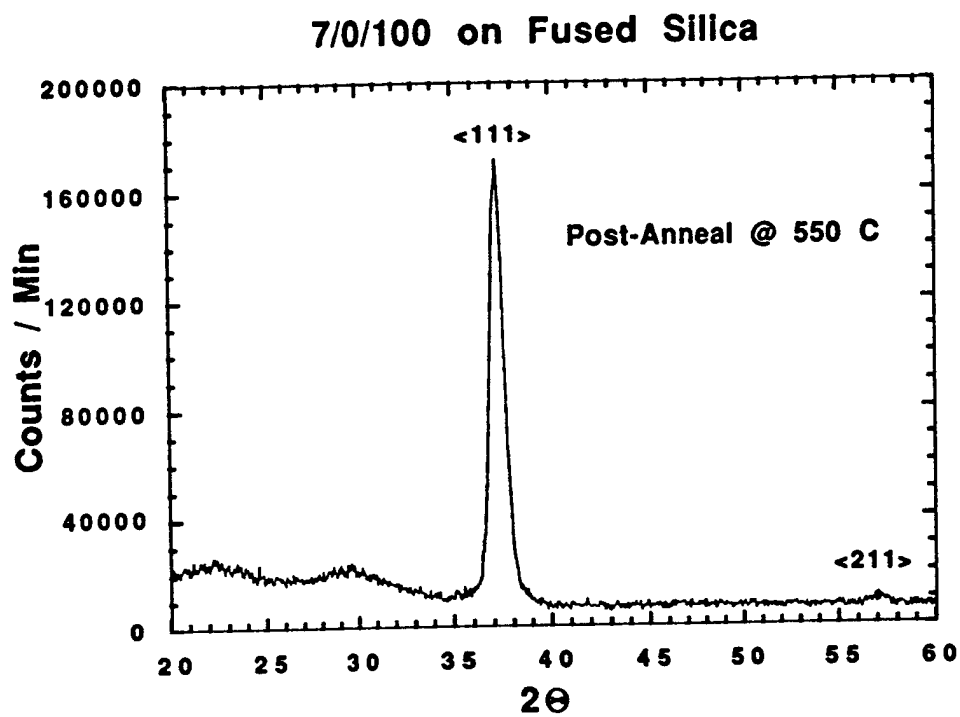
Figure 3.5:   X-Ray Diffraction Pattern of 7/0/100 PLZT on Fused Silica after Post-Anneal @ 550 °C.

7/0/100 @ 450 C on Fused Silica
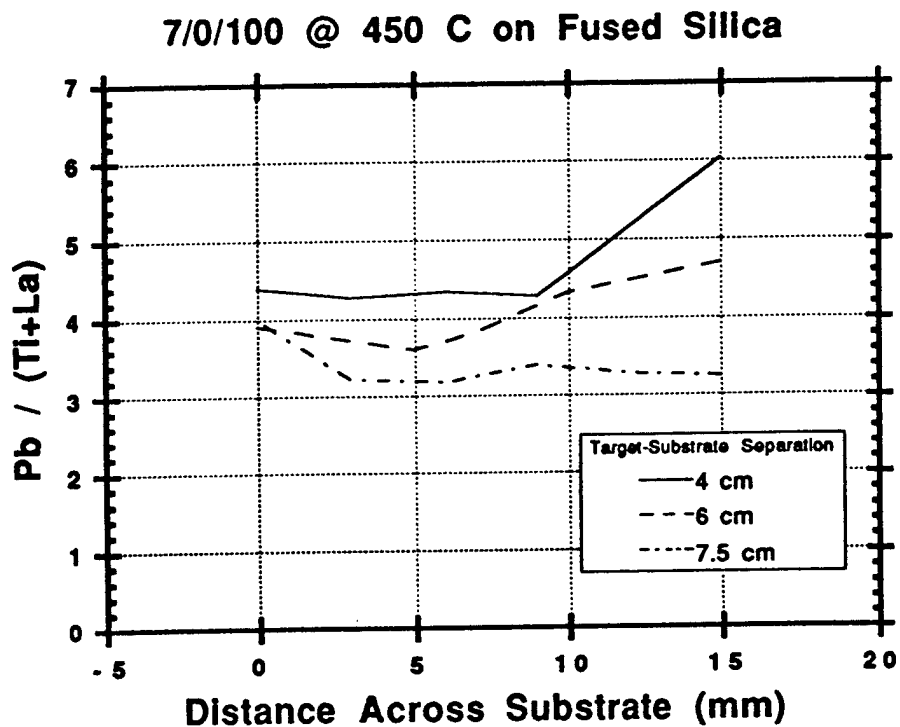
Figure 3.6: 7/0/100 Pb/(Ti+La) Ratios Across the Substrate with Target-Substrate Separation.

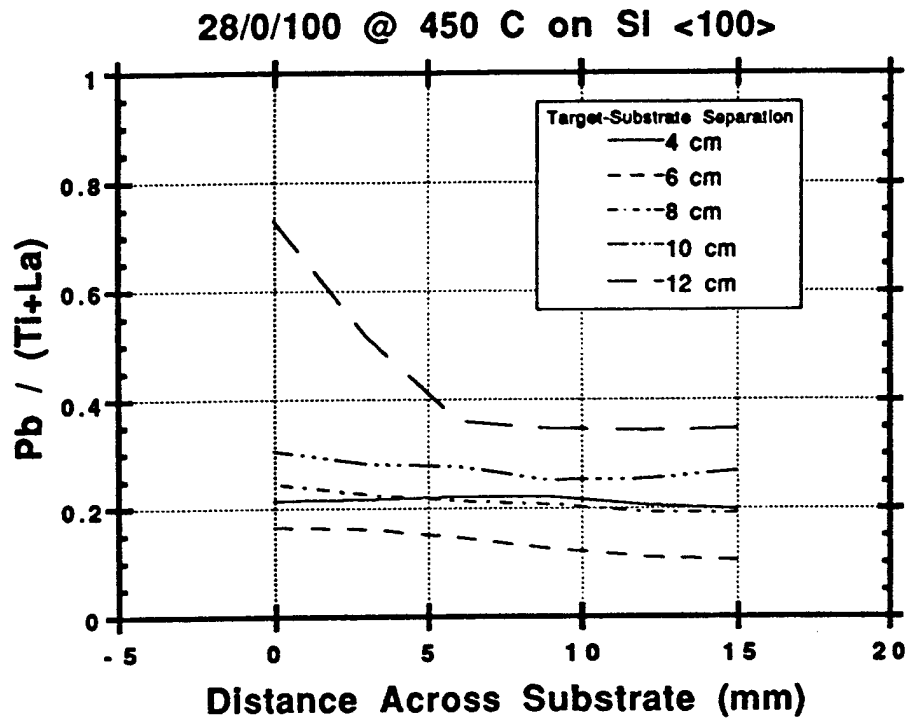**28/0/100 @ 450 C on SI <100>**

Figure 3.7: 28/0/100 Pb/(Ti+La) Ratios Across the Substrate with Target-Substrate Separation.

The Pb/(Ti+La) ratio was evaluated as a function of target-substrate separation. The (7/0/100) samples deposited on fused silica show a decline in Pb/(Ti+La) ratios with increased target-substrate separation. Material of composition (28/0/100) deposited on Si <100> displayed an initial drop in Pb/(Ti+La) ratios from 4 to 6 cm., and a rise in the Pb/(Ti+La) ratios with increased target-substrate separation.

3.2 Oxygen Pressure Investigations

The second part of the investigation examined the stoichiometry as a function of oxygen backfill pressure. Table 2.3 indicates the parameters investigated. During the process of depositing 7/0/100 PLZT for the first part of this investigation, it was noticed that by adjusting the oxygen backfill pressure during deposition, one could control the stoichiometry of the film. In the first part the stoichiometry of the films was controlled by adjusting the substrate temperature, target-substrate separation, and the amount of excess PbO in the target.

The results obtained in depositing PLZT films of composition 7/0/100, 28/0/100, and 0/0/100 onto crystalline Si <100> and amorphous fused silica substrates are presented below. All deposition temperatures ranged from 450-500 °C. A temperature of at least 400 °C is required to promote crystallinity, and a temperature of less than 600 °C is desired for semiconductor processing.

We first examined 7/0/100 PLZT films. Three amounts of excess PbO in the target, 150%, 75%, and 0%, were fixed as the oxygen backfill pressure was varied between 0.1-200 mTorr. Figure 3.8 shows results from these experiments. The Pb/(Ti+La) ratios increase with increasing background oxygen pressure in a logarithmic fashion. Note the decrease in the Pb:Ti ratio with decreasing excess PbO in the target. The proper Pb/(Ti+La) ratio for 7/0/100 PLZT films is $\approx$1.5 to 2.0. Using the information from Figure 3.8 and interpolating, good perovskite PLZT films of 7/0/100 composition can be obtained on Si <100> at $\approx$0.2 to 0.4 mTorr. The film characterized in Figure 3.9 was deposited using an oxygen backfill pressure of 0.2 mTorr and an excess PbO concentration of 75%. The 7/0/100 film stoichiometry closely follows the curve as predicted in Figure 3.8 for the 75% excess PbO composition. The excess PbO targets were chosen due to the ease of obtaining the proper stoichiometry in the 1 mTorr range. After obtaining the desired stoichiometry, the films displayed almost single phase <110> and <111> crystallinity. When deposited on fused silica, higher substrate temperatures and also slightly higher oxygen backfill pressures of 1 mTorr were needed. This produced stoichiometrically correct, single phase crystalline films. By controlling the pressure, a fairly accurate composition (Pb:Ti) can be selected. The results of the 7/0/100 films were considered satisfactory when compared to the predicted values.

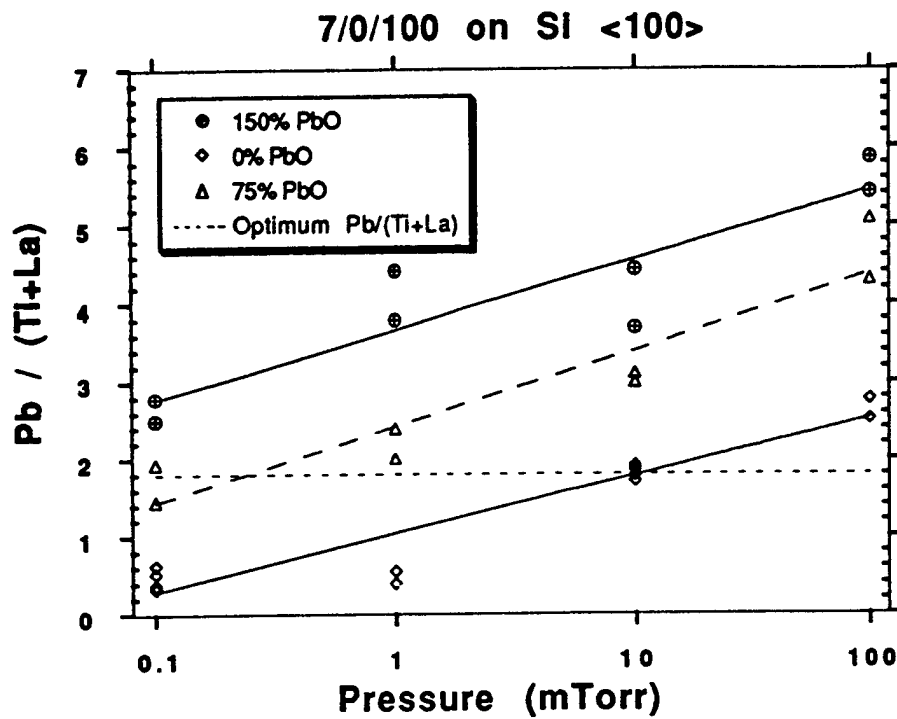**7/0/100 on SI <100>**

Figure 3.8: 7/0/100 PLZT with Various Excess PbO Targets Deposited as a Function of Oxygen Pressure.
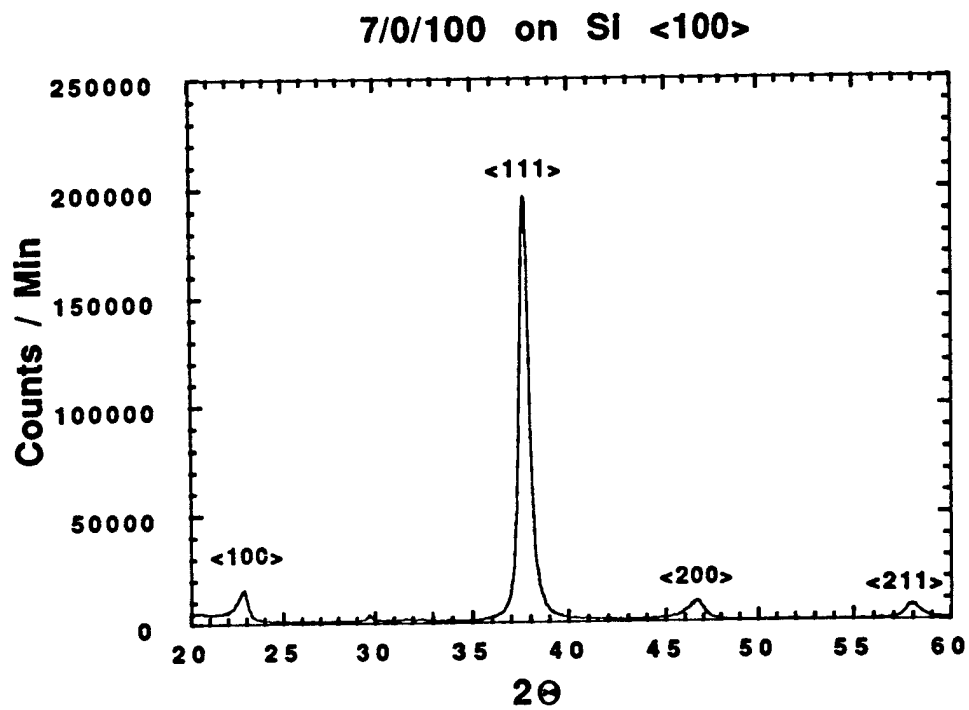
7/0/100 on Si <100>

Figure 3.9: X-Ray Diffraction Pattern of 7/0/100 PLZT on Si <100> @ 500 °C and 0.2 mTorr O_2.

Next the effects of using targets with 75% excess PbO concentrations for producing 28/0/100 films were examined. The substrate temperature was held constant at 500 °C. As the oxygen backfill pressure was varied between 0.1 to 100 mTorr a similar trend as observed in the 7/0/100 films appeared as shown in Figure 3.10. The correct Pb:(Ti+La) ratio for the 28/0/100 films should be ≈2.0. As the oxygen pressure decreased from 1 mTorr to 0.8 mTorr, there was a very apparent sharp drop in the Pb:(Ti+La) ratio. This drop is exemplified in Figure 3.11. Again, the 75% excess PbO targets were used because of the pressure and stoichiometric considerations. Interpolation of data provided proper stoichiometric and perovskite films at an oxygen pressure of ≈0.85 mTorr on Si <100>. The films were predominantly <111> perovskite as seen in Figure 3.12.

Finally, 0/0/100 composition, or lead titanate films were deposited on Si <100> and fused silica. An excess PbO concentration of 75% was used with deposition temperatures of 500 to 530 °C. Data was collected to determine if the drop in the Pb:(Ti+La) ratio also occurred with this composition. Oxygen backfill pressures of 1-10 mTorr were used. Figures 3.13 and 3.14 illustrate this dropoff, but it can be seen that it is not as dramatic as in the 28/0/100 films. Here we see the ratio drop occurs over a range of 1 to 3 mTorr where the 28/0/100 films displayed a ratio drop over approximately 0.2 mTorr. For the
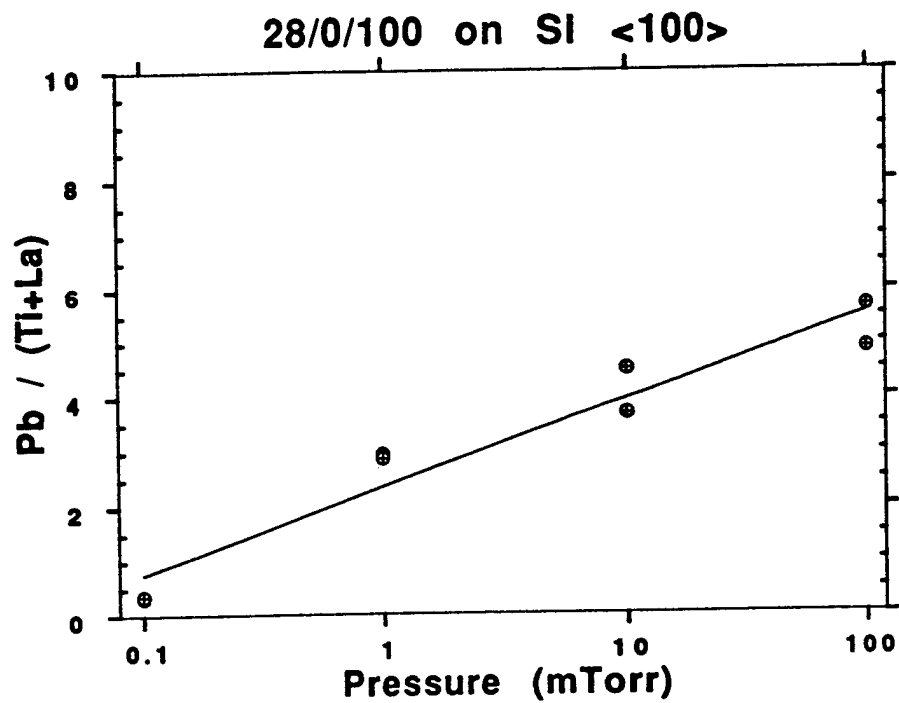
28/0/100 on SI <100>

Figure 3.10: 28/0/100 PLZT Pb/(Ti+La) Ratios

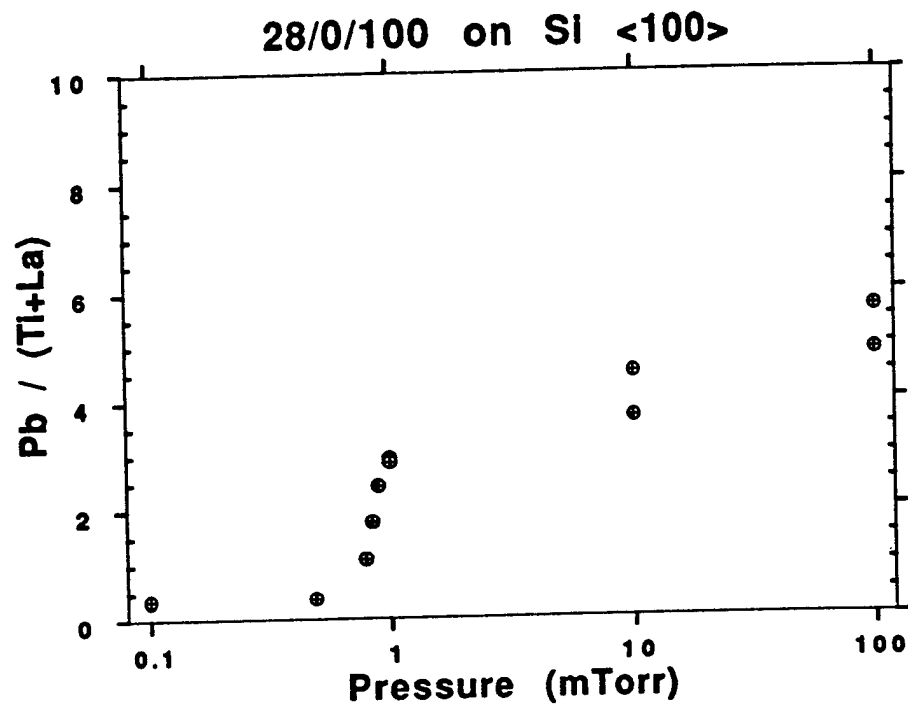**28/0/100 on SI <100>**

Figure 3.11: 28/0/100 PLZT Pb/(Ti+La) Ratios

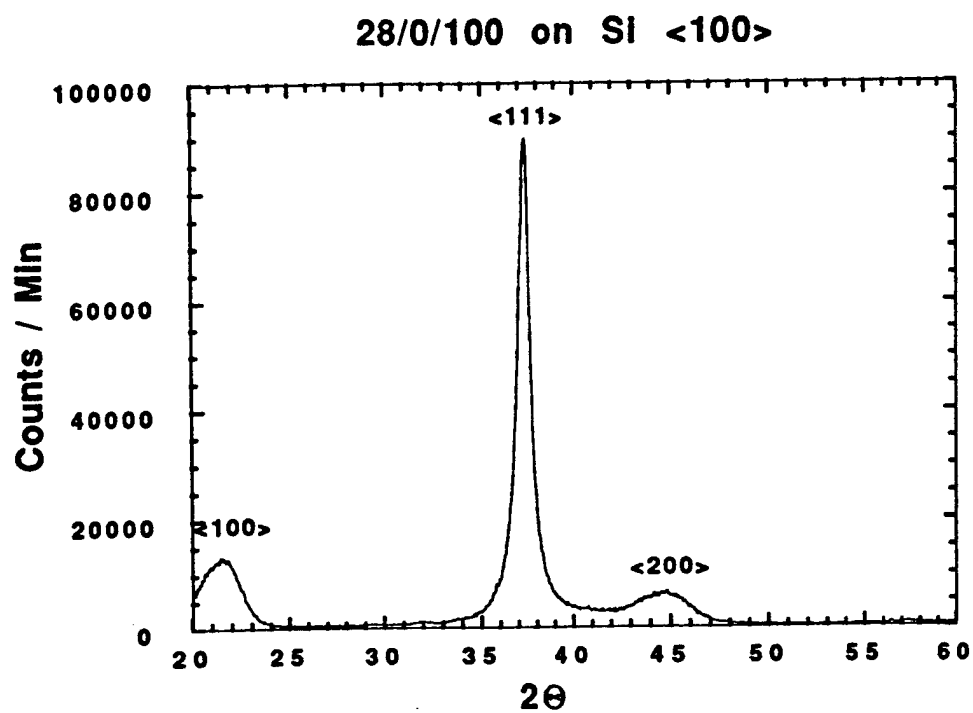**Figure 3.12:** X-Ray Diffraction Pattern of 28/0/100 PLZT on Si <100> @ 500 °C and 0.85 mTorr O_2.
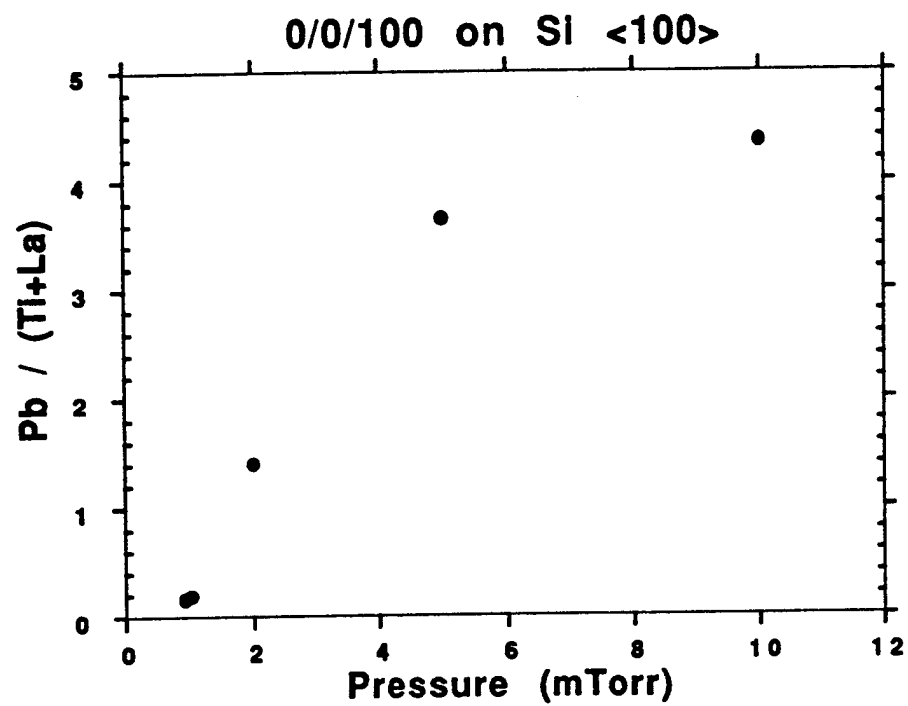
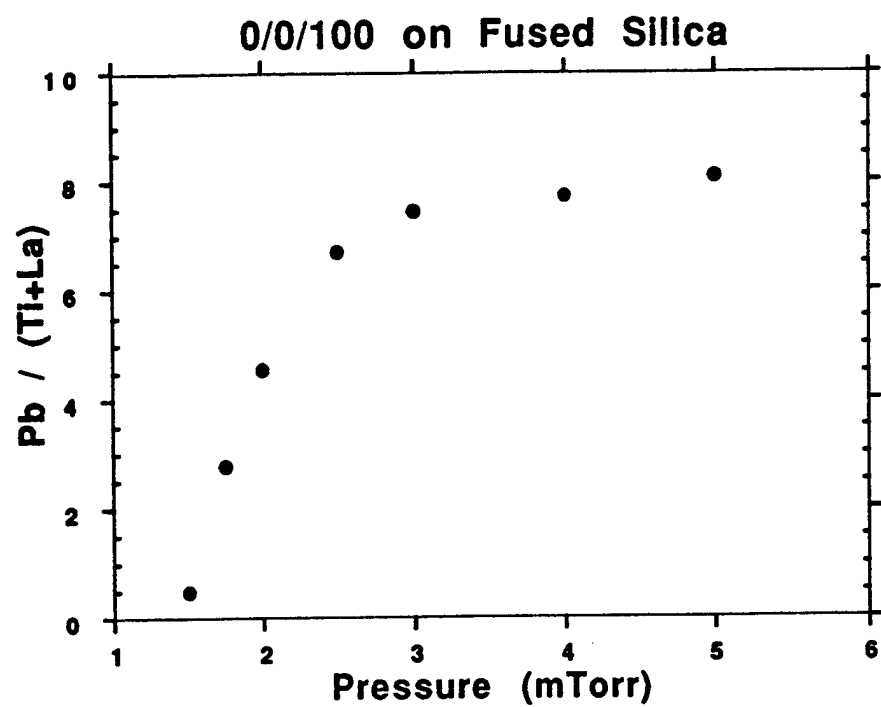Figure 3.13:   0/0/100 PLZT Pb:(Ti+La) Ratios on Si <100>.

Figure 3.14: 0/0/100 PLZT Pb:(Ti+La) Ratios on Fused Silica.

0/0/100 films the Pb:(Ti+La) ratio should be ≈1.0, which is obtained at pressures of ≈1.5 to 1.75 mTorr for 75% excess PbO targets. Proper crystallinity was difficult to obtain in the 0/0/100 PLZT films without a post-annealing process. The onset of crystallinity requires higher energies than available from our deposition. In order to get crystalline films, substrate temperatures ≥600 °C were required. This was not attempted in our deposition system due to high temperature and voltage constraints, thus high quality crystalline <110> perovskite structures were obtained by post-annealing at 600 °C for twenty minutes.

3.3 Grain Size Measurements

Modified lead titanate compositions are polycrystalline materials. Therefore, grains and domains are present in the PLZT thin films. The grain sizes of the laser deposited films were measured using a scanning electron microscope. Figure 3.15 shows a scanning electron micrograph of a 7/0/100 PLZT <110>/<111> mixed phase thin film deposited at 530 °C. The grain sizes exhibited by this film are <0.1 μm. As a comparison, films deposited by ion beam sputtering (see Figure 3.16)[4] have larger grain sizes on the order of 0.1-0.5 μm. It is not known if this is due to the deposition process or the heating schedule. Laser deposited films were heated and cooled to room temperature over a period of one to two hours. In contrast, the ion beam sputtered films were deposited over a period of approximately 20 hours.

Figure 3.15: SEM Micrograph of Laser Deposited 7/0/100 PLZT.

000029 25KV X70.0K 0.43um

Figure 3.16: SEM Micrograph of Ion Beam Sputtered 7/0/100 PLZT.

CHAPTER 4

DISCUSSION

The topics discussed in this section include x-ray diffraction characteristics, film stoichiometric uniformity, oxygen backfill pressure, and grain size.

4.1 X-Ray Diffraction Characteristics

The evaluation of the PLZT material structure requires careful attention to the orientation of the crystallites. The particle size and thickness can cause incomplete cancellation of the incident and refracted x-rays away from the Bragg angle.[4] This cancellation can affect x-ray patterns when examining thin films.

Peak broadening is an effect often observed in x-ray diffraction of thin films. The grain orientation varies slightly in polycrystalline films. This gives rise to multiple 2Θ angles satisfying the Bragg condition, hence peak broadening occurs. A single crystal film would display a sharp, well-defined peak. The broadening occurred in several of the x-ray diffraction results. Peak broadening is also caused by non-uniform strain in the film. This property of x-ray diffraction is often used to identify the types of stress associated with the film. Film stress was not evaluated in this investigation, but may be examined in future work.

The primary use of x-ray diffraction measurements was to determine the material crystalline structure, either perovskite or pyrochlore, and the types of phases present. The aim of the investigation was to produce perovskite PLZT thin films by laser deposition without a post-annealing process. The films of 7/0/100 and 0/0/100 compositions were predominantly perovskite <110>, <111>, or mixed. The 28/0/100 composition films were perovskite <100>, <111>, or mixed. Laser deposition of thin films tends to deposit in the <111> phase. The mechanisms are not understood but may be due to the energies and deposition rates involved. The results indicate no influence of oxygen pressure on the deposited <111> phase. The difference in orientation may be caused by the 28/0/100 composition lying on the cubic and tetragonal phase boundary of PLZT. Further investigation is required in this area.

4.2 Stoichiometric Uniformity

Variation of stoichiometry across the substrate is undesirable. Inhomogeneous compositions, thicknesses, indices of refraction, and crystalline structure occur across the film. The highly directional deposition process of laser ablation produces these inhomogeneities. The limited angular distribution of the plasma plume produces a narrow deposition area and non-uniform deposition. By combining a number of corrective techniques one may be able to coat large areas using laser

49

deposition. One method is rastering the beam on a rotating target, and another is substrate rotation. These methods would allow large parts to be coated with improved stoichiometric and physical uniformity, but may reduce the effective deposition rates.

The results of the target-substrate separation experiments were unexpected. The 7/0/100 results display a decrease in the Pb/(Ti+La) ratio with increasing target-substrate separation. The 28/0/100 films show almost the opposite trend. The 28/0/100 films show an initial drop in the Pb/(Ti+La) ratio from 4 to 6 cm, and an increase from 6 to 12 cm. It is possible that both the 28/0/100 composition and the Si <100> substrate may be related to the cause of this discrepancy, although the actual reason is not understood.

4.3 Oxygen Backfill Pressure

Controlling the oxygen backfill pressure during laser deposition produces desired stoichiometries of PLZT thin films. Perovskite structure is easily obtained with correct stoichiometry.

The amount of lead available to the substrate strongly influences the film quality. Previously, proper stoichiometry was difficult to control due to a high loss of lead. This is presumably caused by a thermal depletion of the target and Pb loss in the

deposited film, caused by re-evaporation of the Pb at the substrate. Hence a low sticking coefficient of Pb results.[21]

The following is a possible explanation of the results obtained from the oxygen pressure investigations. When target material is ablated, Pb atoms exist in a plasma extending a few centimeters from the target surface. If the Pb vapor pressure drops to $\approx 10^{-2}$ to 10^{-4} Torr due to collisions occurring in the plasma, and the oxygen backfill pressure is held constant at a pressure of 10^{-3} Torr, it might be possible for the lead and oxygen atoms to bond together to form lead oxides. If the bond is sufficiently strong, the newly formed molecules may be deposited at the substrate surface. If the molecules have a sufficient sticking coefficient and reduced energy, re-evaporation of the molecules from the substrate will be inhibited. Adequate surface mobility will exist due to an increased substrate temperature, allowing molecules to locate the lowest local potential energy resting site on the substrate surface. Therefore at higher oxygen pressures, 100-200 mTorr, more lead would combine with oxygen and remain on the substrate, which is consistent with the EDS measurements.

The lead-oxygen reaction occurs within the plasma because of the associated mean-free path and reaction rate. Applying concepts from conventional statistical gas kinetic processes, several trends can be observed. The velocity-averaged, gas-

kinetic collision cross section of lead-oxygen might be approximated as[8,40]

$$\sigma_{Pb-O_2} = \pi(r_{Pb} + r_{O_2})^2 \text{ cm}^2, \qquad (4.1)$$

where r_{Pb} and r_{O_2} are the atomic radii of the lead and oxygen respectively. The mean-free path is calculated from the kinetic collision cross-section using[8,40]

$$\lambda_{Pb-O_2} = (n_{O_2}\sigma_{Pb-O_2})^{-1} \text{ cm}^{-1}, \qquad (4.2)$$

where n_{O_2} is the concentration of oxygen molecules. The collision rate is also dependent on the kinetic collision cross-section and is found from[8,40]

$$R_{coll} = [n_{O_2}][n_{Pb}](v)(\sigma_{Pb-O_2}) \quad \text{cm}^{-3}\text{s}^{-1}, \quad (4.3)$$

where n_{Pb} and v are the concentration of lead atoms and the velocity of the lead atoms respectively. Table 4.1 displays the values calculated from these formulae.

The calculated results at a pressure of 1 mTorr indicate a mean-free path between collisions of 0.19 cm and a collision rate of 6×10^{14} cm^{-3}s^{-1}. Even if only 10% of the atoms collide and form lead oxide, it would result in an effective mean free path for Pb-O_2 collisions of 1.9 cm.

Variable	Value
r_{Pb}	1.5 Å
r_{O_2}	3.0 Å
n_{Pb}(42)	10^{10} cm^{-3}
n_{O_2}(8)	3×10^{13} cm^{-3}
σ_{Pb-O_2}	6.4×10^{-15} cm^2
λ_{Pb-O_2}	0.19 cm
v @ 10 eV	3.05×10^5 cm/sec
R_{coll}	6×10^{14} $cm^{-3}s^{-1}$

Table 4.1:   Values and Calculated Results for formulas 4.1, 4.2, and 4.3.

This allows ample opportunities for the lead and oxygen atoms to collide and form molecules within the plasma before reaching the substrate.

Interesting observations were noted with the 28/0/100 and 0/0/100 compositions. At approximately 10^{-3} Torr a sudden and pronounced change occurred in the Pb:(Ti+La) ratios. Examining the ratios of Pb:(Pb+La), Ti:(Pb+La), Pb:(Pb+Ti), La:(Pb+Ti), Pb:La, and Ti:La revealed Pb as the element controlling this change. The lower oxygen backfill pressures may produce smaller amounts of lead oxides and Pb atoms on the substrate surface. This may be due to less oxygen reacting with the Pb, thereby forming less lead oxide. Also, the sticking coefficient of Pb is very low.[21] At higher pressures however, there is a possibility that lead oxides rather than lead atoms are being deposited on the substrate. Evans and Thomas[35] using x-ray photoelectron spectroscopy (XPS) noted at 10^{-3} Torr lead films became completely oxidized as shown in Figure 4.2. Therefore, if a certain threshold oxygen pressure exists where Pb atoms ejected from the target become oxidized, then large amounts of lead oxides and small amounts of elemental lead may be deposited on the substrate. This is a possible explanation for the abrupt change exhibited in the 0/0/100 and 28/0/100 compositions. This change was not noticed in the 7/0/100 compositions, and it is not understood why this occurred. Further investigations of these phenomena require
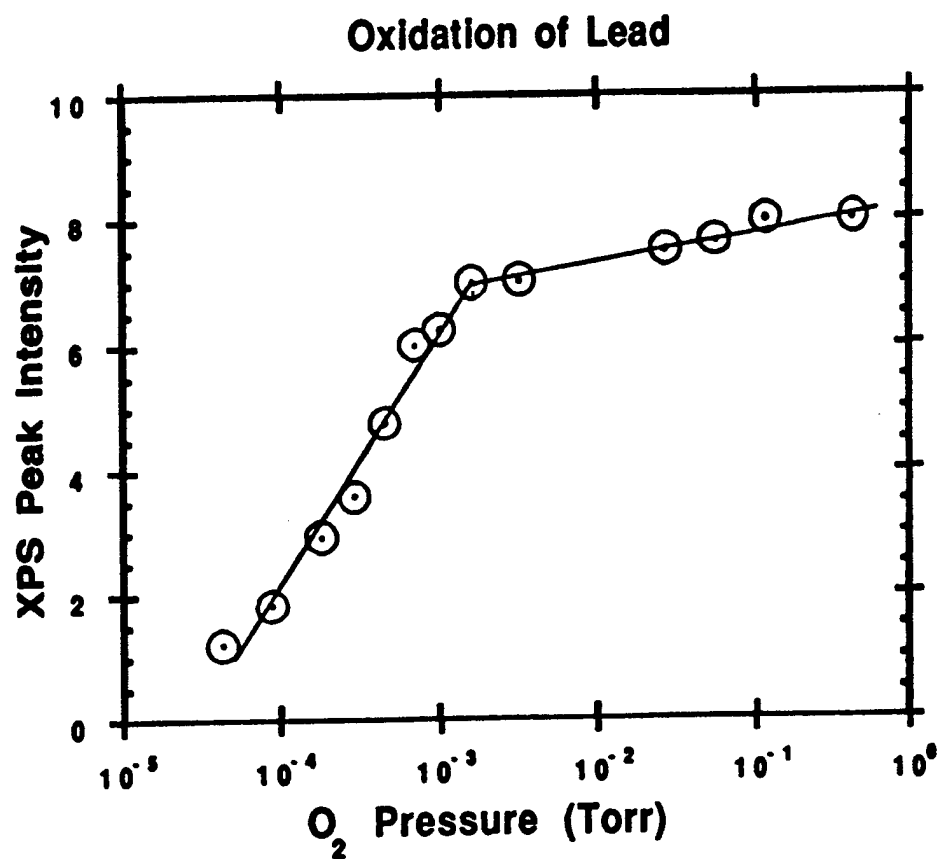
Oxidation of Lead

Figure 4.1: Oxygen Content of Lead Films as a Function of Oxygen Pressure.[35]

the use of XPS or Rutherford Backscattering techniques capable of detecting oxygen in the films.

Another possible explanation of the decrease in lead content in the films with decreased oxygen pressure might be ion or energetic particle bombardment. At low pressures energetic particles may travel out of the plume and impinge on the substrate. This may lead to preferential sputtering of atoms already on the substrate and cause them to be removed.[41] For example, if lead atoms escape the plasma with much of their energy, they might strike the lead atoms in the growing film and remove them via kinetic collisions, as in ion beam sputtering. This would cause thinner films and lower Pb/(Ti+La) ratios as observed. At higher oxygen pressures however, the probability of an energetic particle escaping the plasma is less and hence the chance for preferential sputtering is reduced. Hence thicker films with higher Pb/(Ti+La) ratios would be obtained. This is consistent with observed spectrophotometric results which indicate thicker films are deposited at higher oxygen pressures.

4.4 Grain Size

In general, grain size is most likely dependent on the film deposition technique and/or heating schedule. For example, it has been suggested by Haertling[36] and Yoo et al[37] that grain growth is highly dependent on heating and cooling procedures.

An expression derived by Haertling for grain size in bulk PLZT as a function of time is[36]

$$D = Kt^{1/2}, \qquad (4.4)$$

where D is the grain size, t is the amount of time for heating and cooling, and K is a temperature and material dependent rate constant. If this expression is valid for PLZT thin films, it would explain the grain size discrepancies between magnetron, laser deposited, and ion beam sputtered films due to the heating schedule.[4] Ion beam sputtered films require approximately 20 hour heating cycles whereas other processes take approximately 1-3 hours. The deposition mechanisms themselves may also be partly responsible for the discrepancies, but have not been investigated in this work.

Another possible explanation of the differences encountered is given by Yoo et al.[37] Their work suggests chemical reactions between the PbO, TiO_2, and La_2O_3 combine to form PLZT at slow deposition and heating rates. Faster deposition processes may result in incomplete reactions between the constituent oxides, improper structure, and smaller grains. Also, improper stoichiometric ratios results in decomposition of grain inducing elements thereby reducing or inhibiting grain growth.[4] This may explain why proper stoichiometry leads to correct crystal structure. Much more additional work, beyond the scope of this thesis, is required to explain grain size phenomena exhibited by different deposition techniques.

CHAPTER 5

CONCLUSIONS

Fabrication of PLZT thin films requires deposition techniques capable of producing highly oriented and stoichiometrically correct films. In this investigation laser ablation was demonstrated to be a novel and excellent technique for producing high quality PLZT thin films. The ability shown by the laser ablation processb to deposit stoichiometrically correct, highly oriented material without a post-annealing process is very desirable. Also, by controlling the backfill oxygen pressures and the amounts of excess PbO in the targets, better quality films can be deposited. This can be very beneficial for the use of PLZT thin films in optical, electrical, and electrooptic applications.

Stoichiometrically correct PLZT thin films of composition 0/0/100, 7/0/100, and 28/0/100 can be laser deposited with a perovskite crystalline structure. The films are comparable in quality to those deposited by magnetron and ion beam sputtering. The results also indicate several areas which should be further investigated.

One area of future investigation is to better quantify the amounts of Pb and PbO_x in the deposited films. This entails the use of XPS and/or RBS measurements of oxygen or oxides in the

deposited films. Determining the role lead oxidation plays in PLZT thin film deposition processes is very interesting. Because Pb seems to be the controlling factor in determining the correct composition of the film during deposition, Pb and PbO_x measurements would be extremely beneficial in better understanding the deposition process.

Another area of future investigation is the effects of both deposition technique and heating schedule on film grain growth. Both have been shown to exhibit effects on grain growth, but the reasons are not well understood. Much work can be done to explain these phenomena.

Finally, further work is needed in developing a system to deposit stoichiometrically uniform films over large areas using laser ablation. One could also investigate the target-substrate separation effects on different compositions, and the mechanisms behind the preferred crystal orientations in the different compositions. All of these ideas would yield interesting information that would help to enhance future PLZT thin film production and quality.

REFERENCES

1. G.H. Haertling, J. Amer. Cer. Soc. **54**, 303 (1971).

2. T. Nakagawa, J. Yamaguchi, T. Usuki, Y. Matsui, M. Okuyama, and Y. Hamakawa, Jap. J. Appl. Phys. **18**, 897 (1979).

3. M. Okuyama, T. Usuki, Y. Hamakawa, and T. Nakagawa, Appl. Phys. **21**, 339 (1980).

4. L.L. Boyer "Ion Beam Sputtering of Electrooptic PLZT Thin Films" MSEE Thesis, University of New Mexico (1990).

5. H.R. Kaufman, J.J. Cuomo, and J.M.E. Harper, J. Vac. Sci. Technol. **21**, 725 (1982).

6. J.M.E. Harper and J.J. Cuomo, J. Vac. Sci. Technol. A **1**, 37 (1983).

7. C.E. Land, P.D. Thacher, and G.H. Haertling, <u>Applied Solid State Science</u>, v. 4, p. 137, Academic Press, New York (1983).

8. J.R. McNeil "Thin Films and Plasma Processing" EECE 595 class notes, University of New Mexico (Spring 1990).

9. F.L. Williams, J.J. McNally, G.A. Al-Jumaily, and J.R. McNeil, J. Vac. Sci. Technol. A **5**, 2159 (1987).

10. Y. Hamakawa, Y. Matsui, Y. Higuma, and T. Nakagawa, Tech. Digest IEEE IEDM, p.297, Washington, DC (1977).

11. W.E Perry and B.M. Soltoff, Ferroelectrics **10**, 201 (1976).

12. S.G. Varnado and W.D. Smith, IEEE J. Quantum Electronics **QE-8**, 88 (1972).

13. C.E. Land and W.D. Smith, Appl. Phys. Lett. **23**, 57 (1973).

14. A. Kumada, K. Suzuki, and G. Toda, Ferroelectrics **10**, 25 (1976).

15. R.N. Castellano, M.R. Notis, and G.W. Simmons, Vacuum **27**, 109 (1977).

16. D. Berlincourt and H.H.A. Krueger, J. Appl. Phys. **30**, 1804 (1959).

17. J.C. Pivin, J. Mater. Sci. **18**, 1267 (1983).

18. P.E Dyer, R.D. Greenough, A. Issa, and P.H. Key, Appl. Phys. Lett. **53**, 534 (1988).

19. J.P. Zheng, Z.Q. Huang, D.T. Shaw, and H.S. Kwok, Appl. Phys. Lett. **54**, 280 (1989).

20. R.C.Estler, S. Foltyn, A.R. Garcia, R.E. Meunchausen, N.S. Nogar, and M. Trkula, Materials and Manufacturing Processes **5**, 529 (1990).

21. G.A. Petersen, L.C. Zou, W.M. VanBuren, L.L. Boyer, and J.R. McNeil, Proc. Materials Research Society 1990 Spring Meeting. Vol. 200, p.127, San Francisco, CA (1990).

22. C.R. Giuliano, Appl. Phys. Lett. **5**, 137 (1964).

23. H.M. Smith and A.F. Turner, Appl. Opt. **4**, 147 (1965).

24. H. Sankur and J.T. Cheung, Appl. Phys. **A47**, 271 (1988).

25. J.T. Cheung and H. Sankur, CRC Crit. Rev. Sol. St. Mater. Sci. **15**, 63 (1988).

26. C.B. Collins, F. Devanloo, E.M. Jeungerman, W.R. Osborn, and D.R. Jander, Appl. Phys. Lett. **54**, 216 (1989).

27. X.D. Wu, D. Dijkkamp, S.B. Ogale, A. Inam, E.W. Chase, P.F.Miceli, C.C. Chang, J.M. Taracson, and T. Venkatesan, Appl. Phys. Lett. **51**, 861 (1987).

28. D. Dijkkamp, T. Venkatesan, X.D. Wu, S.A. Saheen, N. Jisrani, Y.H. Min-Lee, W.L. Mclean, and M. Croft, Appl. Phys. Lett. **51**, 619 (1987).

29. H.S. Kwok, P. Mattocks, L. Shi, X.W. Wang, S. Witanachchi, Q.Y. Ying, J.P. Zheng, and D.T. Shaw, Appl. Phys. Lett. **52**, 1825 (1988).

30. N.S. Nogar, R.C. Estler, and C.M. Miller, Anal. Chem. **57**, 2441 (1985).

31. T. Venkatesan, X.D. Wu, A. Inam, and J.B. Wachtman, Appl. Phys. Lett. **52**, 1193 (1988).

32. R. Kelley and R.W. Dreyfus, Surf. Sci. **198**, 263 (1988).

33. R. Kelley and R.W. Dreyfus, Nuc. Instr. Meth. Phys. Res. B **32**, 341 (1988).

34. E.A. Brandes, ed. <u>Smithell's Metals Reference Book 6</u>[th] <u>Edition</u>, p. 8-53, Butterworth & Co., Ltd., London (1983).

35. S. Evans and J.M. Thomas, J. Chem. Soc. Faraday Trans. I **71**, 313 (1974).

36. G.H. Haertling, J. Amer. Cer. Soc. **49**, 113 (1966).

37. Y.S. Yoo and J.J. Kim, J. Amer. Cer. Soc. **70**, C322 (1987).

38. L.L. Boyer, A.Y. Wu, G.W. Metzger, and J.R. McNeil, J. Vac. Sci. Technol. A **7**, 1199 (1989).

39. A. Mukherjee, S.R.J. Brueck, and A.Y. Wu, Opt. Comm. **76**, 220 (1990).

40. E.W. McDaniel, <u>Collision Phenomena in Ionized Gases</u>, John Wiley & Sons, Inc., New York (1964).

41. J.B. Malherbe, S. Hofmann, and J.M. Sanz, Appl. Surf. Sci. **27**, 355 (1986).

42. R. Koppmann, S.M. Refaei, and A. Pospieszczyk, J. Vac. Sci. Tech. A **4**, 79 (1986).

43. R. Jenkins, et al., <u>Powder Diffraction File 2: Inorganic Phases.</u>, (Joint Committee on Powder Diffraction Standards International Centre For Diffraction Data, Swarthmore, PA, 1988).